SUPPLEMENTAL DATA

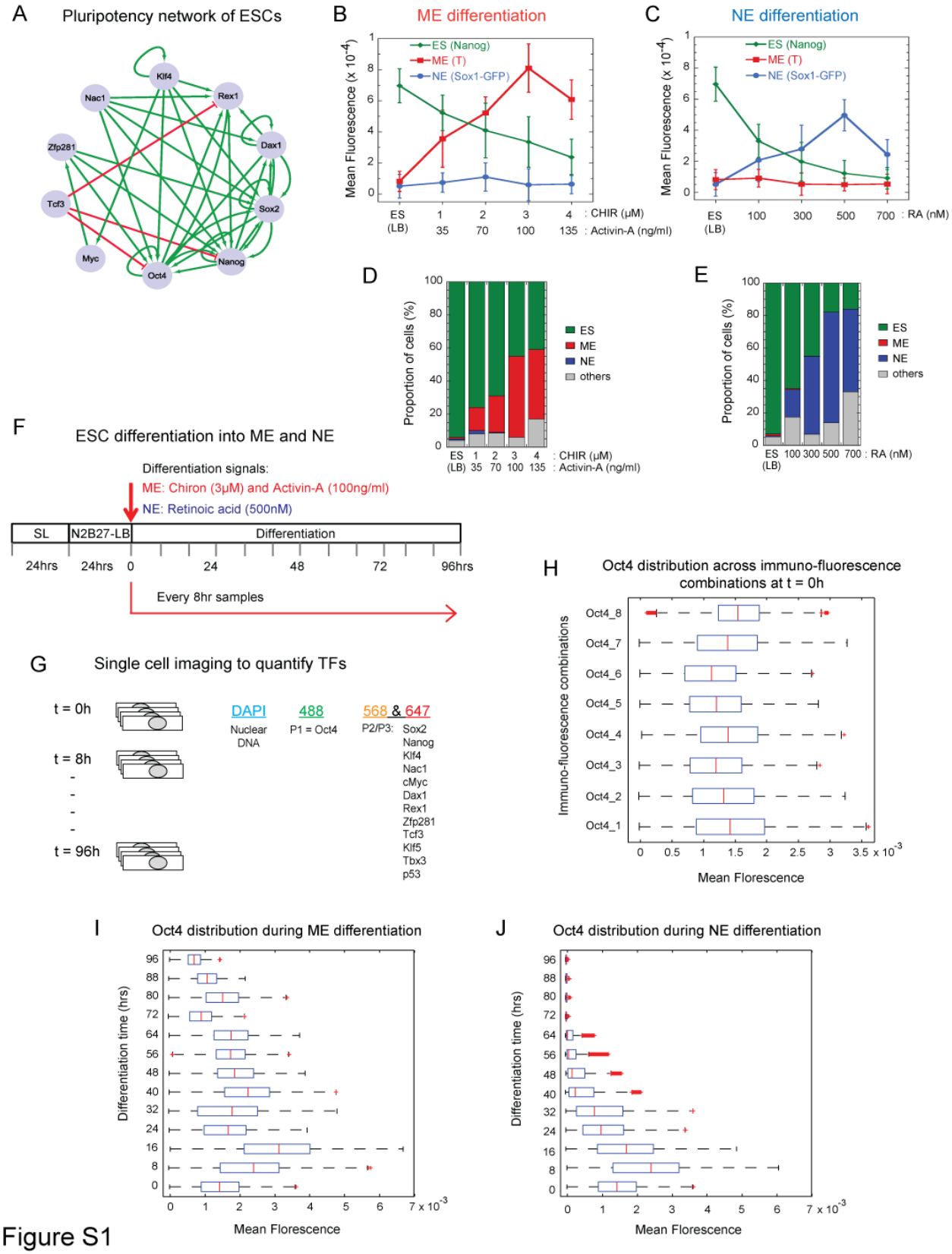

Figure S1

Figure S1: ESC differentiation into ME and NE cell fates and quantification of TF levels. Related to Figure 1.

The pluripotency of ESCs is maintained by an ensemble of interlinked TFs (Chen et al., 2008; Cole et al., 2008; Dunn et al., 2014; Kim et al., 2008; MacArthur et al., 2012) (A). The network is redrawn from Kim et al (Kim et al., 2008) to show the regulatory relationships among the key nine members of the extended pluripotency network, and to incorporate Tcf3-mediated inhibition of Nanog, Oct4 and Rex1 (Cole et al., 2008; Pereira et al., 2006; Wray et al., 2011). Green and red arrows indicate activation and inhibition, respectively, through gene regulation.

Changes in mean fluorescence intensity of Nanog, T and Sox1-GFP at increasing concentrations of CHIR and Activin (B) and Retinoic acid (RA) (C). Changes in the proportion of ES, ME and NE cells at increasing concentrations of CHIR and Activin (D) and Retinoic acid (RA) (E). The error bars show the standard deviation from triplicate measurements. (F) Overview of the method and sample collection for ESC differentiation into either the ME and NE cell fates. ESCs were kept in serum plus leukemia inhibitory factor (LIF) (SL) for 24 hrs, which was replaced with basal N2B27 supplemented with LIF and Bmp4 (LB) for 24 hrs; cells were then washed and the medium was replaced with fresh N2B27 without LIF and BMP but containing either ME- or NE-specific differentiation signals. Cell populations were collected for quantitative immuno-fluorescence at time periods 0, 24, 32, 40, …, 120 hrs for fate marker analysis shown in Figure 1B and C, and every 8 hrs up to 96 hrs for TF analysis shown in Figure 1D and E.

(G) In each immuno-fluorescence experiment, up to three proteins were stained using the primary antibody against each protein and the host-specific secondary antibody conjugated with one of the Alexa-fluor 488, 568 and 647 fluorophores. As a fourth channel, nuclear DNA was stained using DAPI. Multiple combinations of three proteins were chosen to accommodate all 13

proteins (P) measured; Oct4 was kept common (as P1 in the 488 channel) across all combinations; as P2 and P3, the 568 and 647 channels were used, respectively, to immuno-stain the remaining 12 proteins in various combinations.

(H) Box plots showing single-cell distributions of Oct4 in pluripotent cells (differentiation time = 0h) from multiple immuno-fluorescence combinations, as described in (G), confirming the reproducibility of data across multiple stainings.

(I) & (J) Box plots showing single-cell distributions of Oct4, as one representative of the 13 proteins being analyzed, during the ME and NE differentiation process, respectively, at the indicated time points from 0 to 96 hrs.

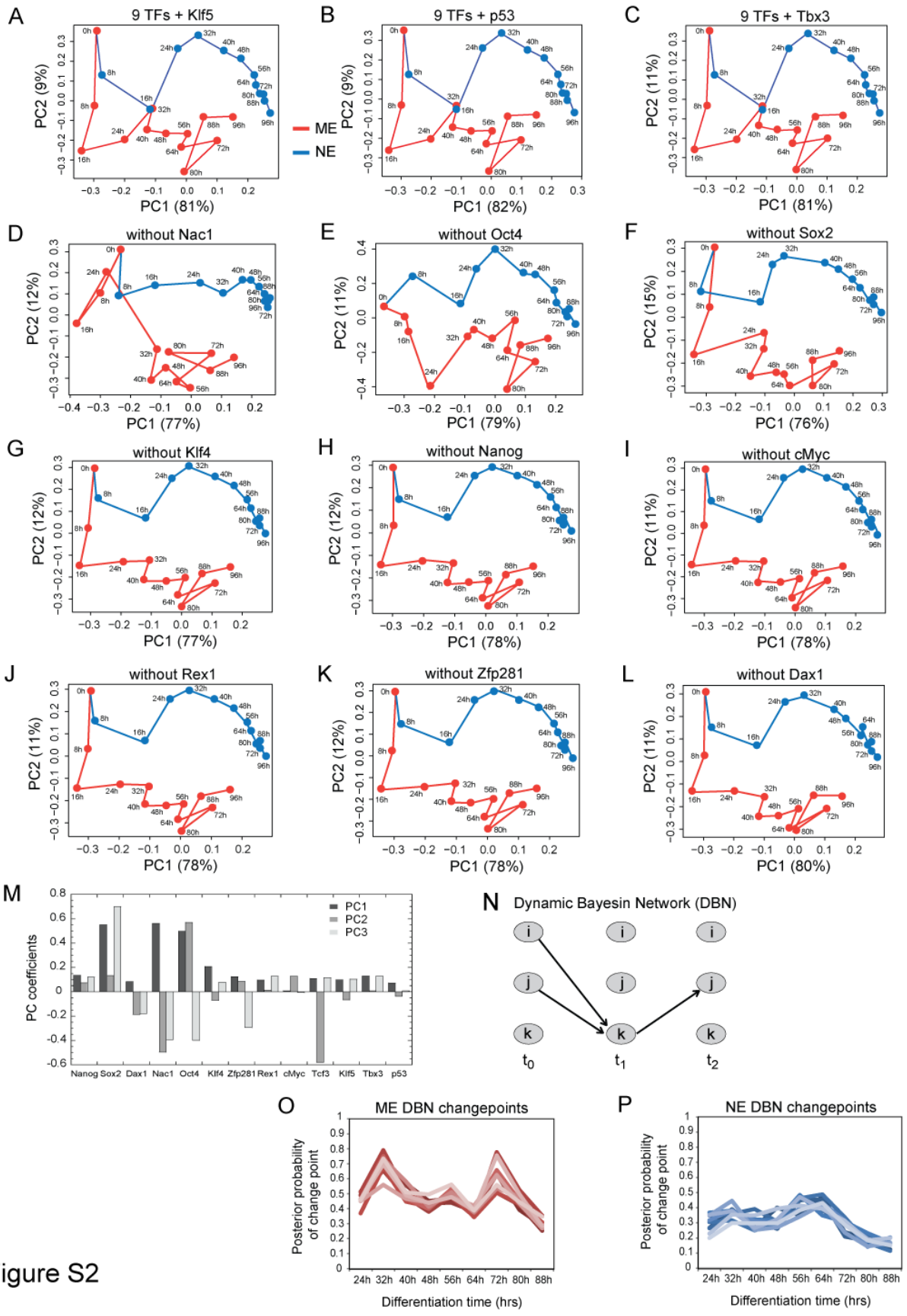
A
9 TFs + Klf5
B
9 TFs + p53
C
9 TFs + Tbx3
ME
NE
PC1 (81%)
PC2 (9%)
PC1 (82%)
PC2 (9%)
PC1 (81%)
PC2 (11%)
D
without Nac1
E
without Oct4
F
without Sox2
PC1 (77%)
PC2 (12%)
PC1 (79%)
PC2 (11%)
PC1 (76%)
PC2 (15%)
G
without Klf4
H
without Nanog
I
without cMyc
PC1 (77%)
PC2 (12%)
PC1 (78%)
PC2 (12%)
PC1 (78%)
PC2 (11%)
J
without Rex1
K
without Zfp281
L
without Dax1
PC1 (78%)
PC2 (11%)
PC1 (78%)
PC2 (12%)
PC1 (80%)
PC2 (11%)
M
PC1
PC2
PC3
PC coefficients
Nanog Sox2 Dax1 Nac1 Oct4 Klf4 Zfp281 Rex1 cMyc Tcf3 Klf5 Tbx3 p53
N
Dynamic Bayesin Network (DBN)
i
j
k
t0
t1
t2
O
ME DBN changepoints
Posterior probability of change point
Differentiation time (hrs)
P
NE DBN changepoints
Posterior probability of change point
Differentiation time (hrs)

Figure S2

Figure S2: Principal component analysis and dynamic Bayesian network to identify key regulators of differentiation. Related to Figure 2.

PCA analysis of temporal data of ten TFs by inclusion of either Klf5 (A), p53 (B) or Tbx3 (C) to the data from nine TFs - Oct4, Nanog, Sox2, Klf4, Rex1, Nac1, Zfp281, Dax1 and cMyc.

PCA analysis by exclusion of indicated TF from the ten TFs (above nine plus Tcf3): Nac1 (D), Oct4 (E), Sox2 (F), Klf4 (G), Nanog (H), cMyc (I), Rex1 (J), Zfp281 (K) and Dax1 (L).

(M) Contribution of each of the 13 TFs to the first three PCs are shown as PC coefficients.

(N) Dynamic Bayesian Network (DBN) schematic: ***i***, ***j*** and ***k*** represent nodes (TFs in our case) at successive time points; t_0, t_1 and t_2. Arrows in a Bayesian network indicate potential causal relationships between nodes. A DBN adds the element of time and allows protein levels at time point 't' to causally depend on protein levels at time point 't-1' (arrows). The causalities implemented by the arrows are described by joint probability distributions which are chosen to best account for the observed correlations in the data. (O and P) Changes to posterior probability from time t to t-1 for ME and NE from DBN analysis of differentiation data for ten TFs - Oct4, Nanog, Sox2, Klf4, Rex1, Nac1, Zfp281, Dax1, cMyc and Tcf3. The first three and the last time points (0h, 8h, 16h and 96h), which are not shown in the plots, were used to assist the DBN algorithm to recognize the initial and final states of the network. The peaks at 32hrs indicate the maximum changes observed (from 0 to 0.8 for ME and 0 to 0.4 for NE). Although additional major peaks are observed, at 72hrs for ME and 64hrs for NE, the posterior probability change between these times and their previous time (64hrs for ME and 56hrs for NE) are much smaller. The shades within ME and NE indicate results from repeated and independent runs of the DBN analysis. Further details of DBN analysis are described in the Supplemental Procedures.

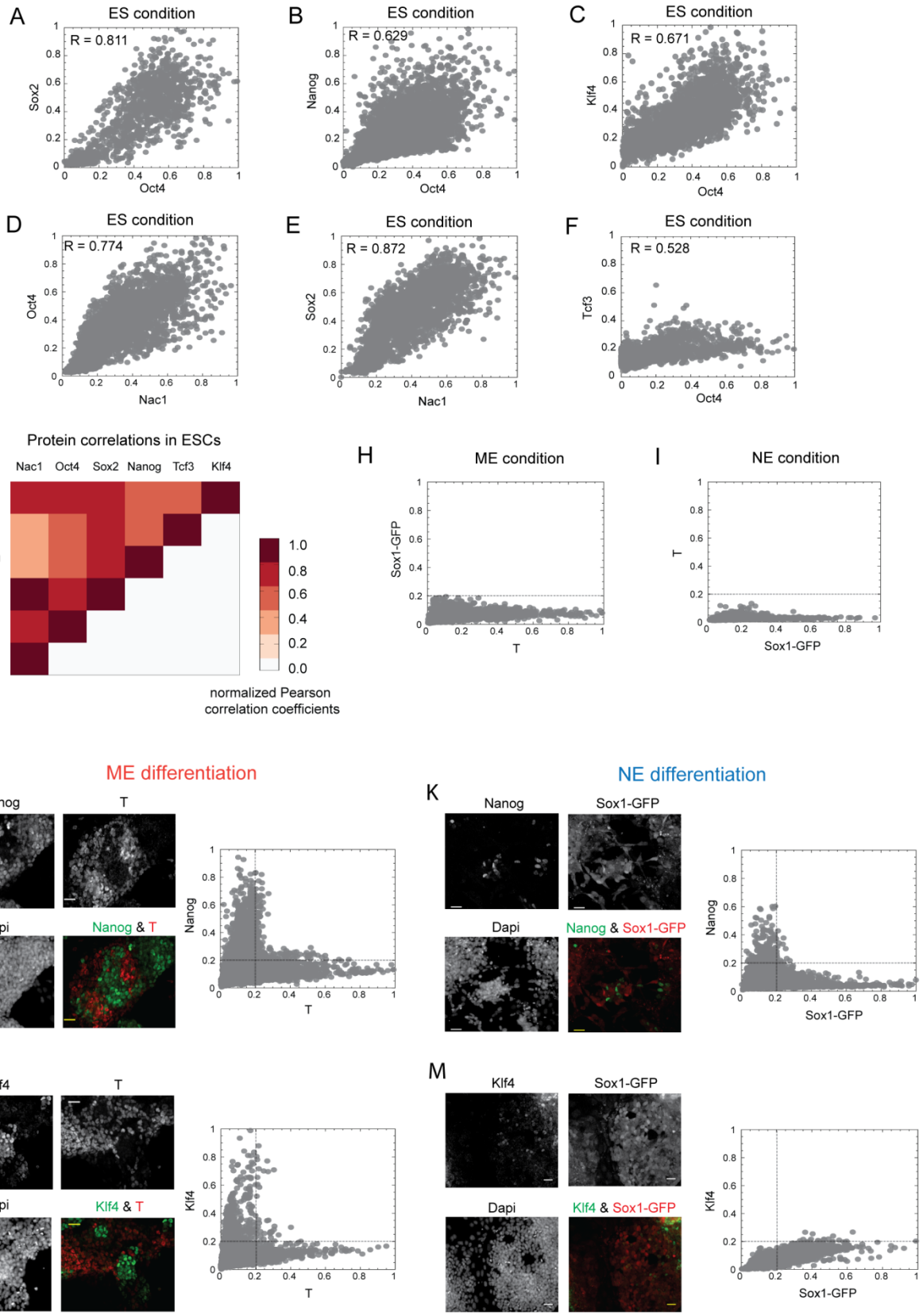
A
ES condition
R = 0.811
Sox2
Oct4
B
ES condition
R = 0.629
Nanog
Oct4
C
ES condition
R = 0.671
Klf4
Oct4
D
ES condition
R = 0.774
Oct4
Nac1
E
ES condition
R = 0.872
Sox2
Nac1
F
ES condition
R = 0.528
Tcf3
Oct4
G
Protein correlations in ESCs
Nac1 Oct4 Sox2 Nanog Tcf3 Klf4
Klf4
Tcf3
Nanog
Sox2
Oct4
Nac1
1.0
0.8
0.6
0.4
0.2
0.0
normalized Pearson correlation coefficients
H
ME condition
Sox1-GFP
T
I
NE condition
T
Sox1-GFP
J
ME differentiation
Nanog
T
Dapi
Nanog & T
Nanog
T
K
NE differentiation
Nanog
Sox1-GFP
Dapi
Nanog & Sox1-GFP
Nanog
Sox1-GFP
L
Klf4
T
Dapi
Klf4 & T
Klf4
T
M
Klf4
Sox1-GFP
Dapi
Klf4 & Sox1-GFP
Klf4
Sox1-GFP

Figure S3

Figure S3: Single cell quantitative pattern of key TFs in ES, ME and NE conditions. Related to Figure 3.

Scatter plots for Oct4 and Sox2 (A); Oct4 and Nanog (B); Oct4 and Klf4 (C); Nac1 and Oct4 (D); Nac1 and Sox2 (E); and, Oct4 and Tcf3 (F) under the ES condition. Pearson correlation coefficients (R) from a linear fit are shown. Indicated TF levels (except Tcf3) were normalized to their single cell maximum under the ES condition as explained in the main text and Supplemental Procedures. Since Tcf3 levels were maximal in NE condition, its levels was normalized to its maximum in the NE condition. (G) Heatmap of pair-wise correlations among the indicated six TFs identified in the computational data analysis. Normalized Pearson correlation coefficients observed with protein levels in ES condition are shown.

Scatter plots for T and Sox1-GFP, under ME (H) and NE (I) differentiation conditions. Chiron (Wnt3a agonist) with Activin-A exclusively induced ME fate choice and retinoic acid exclusively induced the NE choice. Qualitative images (left) and quantitative single cell measurements (right) for Nanog (J & K) and Klf4 (L & M) in ME and NE differentiation conditions. The TFs and T were immuno-stained in the Sox1-GFP ES cell line. Max-normalized fluorescence intensities of Nanog and Klf4 against the T (ME marker) and Sox1-GFP (NE marker) levels are shown. For comparative purposes, fate marker signals were normalized across all conditions (i.e. ME and NE) by their maximum in the respective differentiation condition – ME for T and NE for Sox1-GFP. Similarly Nanog and Klf4 signals were normalized across all conditions by their maximum under ES condition. Cells were fixed, stained and measurements were done at 72 hrs of differentiation. Scale bars represent 35 μm.

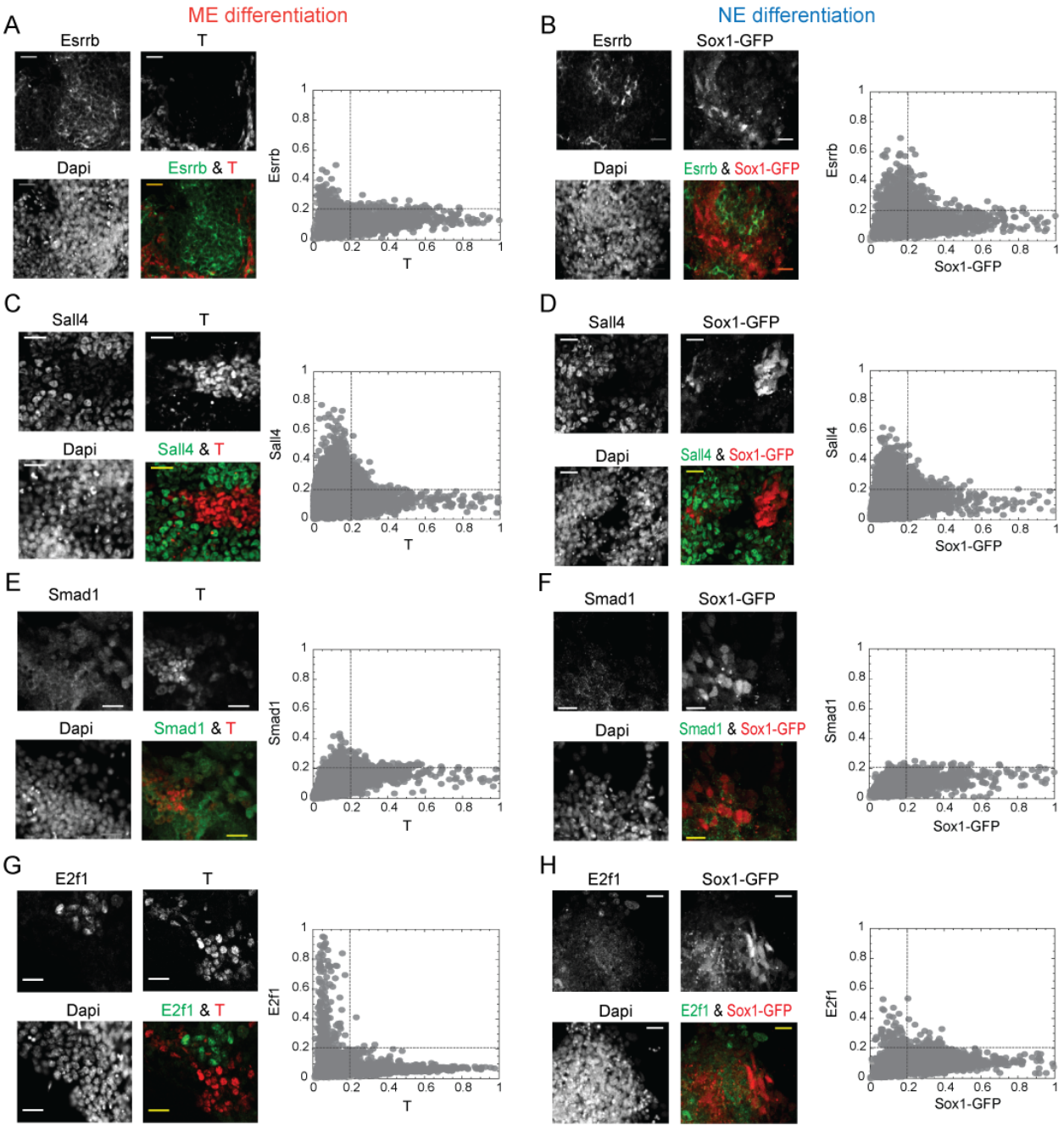

Figure S4

Figure S4: Differential expression of additional TFs in ME & NE cells. Related to Figure 3.

Qualitative images (left) and quantitative single cell measurements (right) for Esrrb (A & B), Sall4 (C & D), Smad1 (E & F), and E2f1 (G & H) in ME and NE differentiation conditions. Measurements and normalizations were performed as in figure S3. Scale bars represent 50μm.

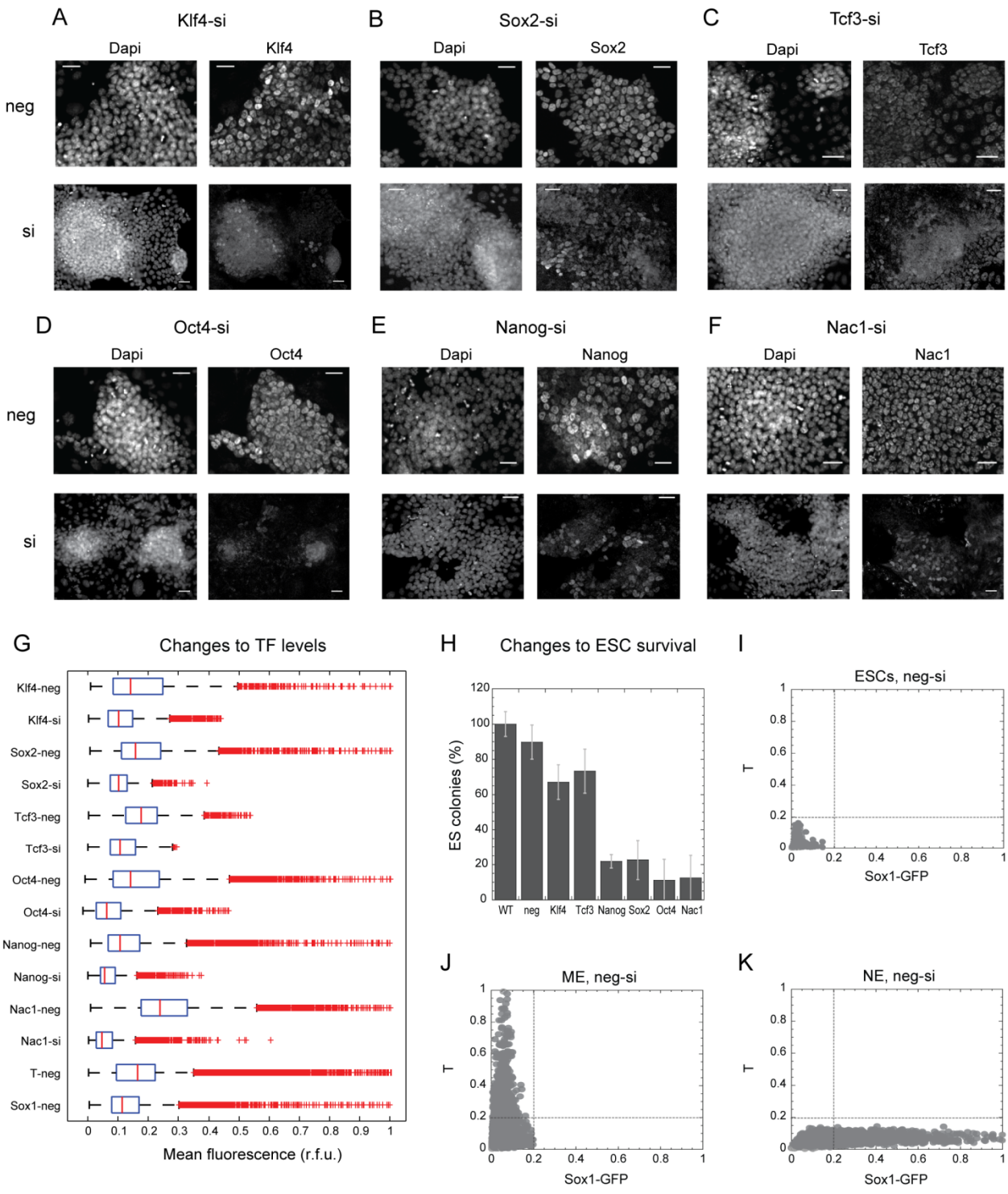
A
Klf4-si
Dapi
Klf4
neg
si
B
Sox2-si
Dapi
Sox2
C
Tcf3-si
Dapi
Tcf3
D
Oct4-si
Dapi
Oct4
E
Nanog-si
Dapi
Nanog
F
Nac1-si
Dapi
Nac1
G
Changes to TF levels
Klf4-neg
Klf4-si
Sox2-neg
Sox2-si
Tcf3-neg
Tcf3-si
Oct4-neg
Oct4-si
Nanog-neg
Nanog-si
Nac1-neg
Nac1-si
T-neg
Sox1-neg
0 0.1 0.2 0.3 0.4 0.5 0.6 0.7 0.8 0.9 1
Mean fluorescence (r.f.u.)
H
Changes to ESC survival
ES colonies (%)
0 20 40 60 80 100 120
WT neg Klf4 Tcf3 Nanog Sox2 Oct4 Nac1
I
ESCs, neg-si
T
Sox1-GFP
0 0.2 0.4 0.6 0.8 1
J
ME, neg-si
T
Sox1-GFP
K
NE, neg-si
T
Sox1-GFP

Figure S5

Figure S5: Tests of siRNAs for down-regulating the TF levels and on ES survival. Related to Figure 4.

Immuno-fluorescence images of ESCs transfected with either scrambled siRNA (neg) or indicated target specific siRNA pool for Klf4 (A), Sox2 (B), Tcf3 (C), Oct4 (D), Nanog (E) and Nac1 (F). Cells were transfected with 25 nM of the indicated gene-specific siRNA pool, maintained under ES condition for 72 hrs, and then fixed and immuno-stained. Scale bars represent 35μm. (G) Box plots showing the distributions of single cell quantifications for changes in the indicated TF levels when ESCs were transfected with either scrambled siRNA (neg) or target specific siRNA pool. (H) Proportion of proliferating ESCs (colonies) upon transfection with either scrambled siRNA (neg) or the indicated target specific siRNA pool. ES colonies were stained for alkaline phosphatase after six days of siRNA transfection. WT: wild type, non-transfected ESCs. The error bars show the standard deviation from triplicate measurements. Sox1-GFP and T scatter plot for single cells upon transfection of ESCs with scrambled siRNA (neg-si) during no differentiation (ES condition) (I), during ME differentiation (J) and during NE differentiation (K). Single cell quantifications were performed at 72 hrs post transfection. In G and I – K, single cell signals are normalized to the maximal signal observed from non-transfected ESCs under the ES (for TFs), ME (for T) or NE (for Tcf3 and Sox1) conditions.

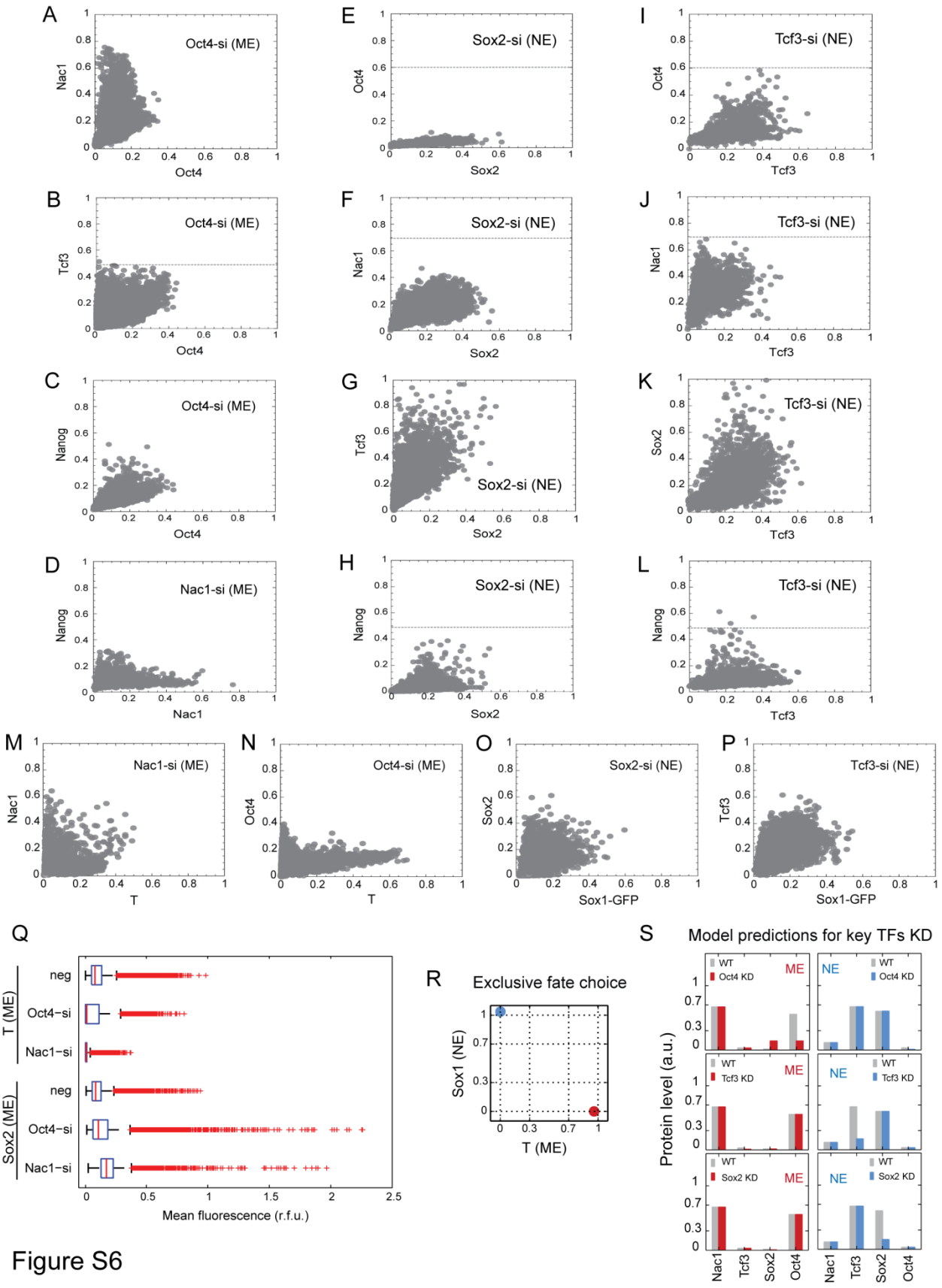
A
Oct4-si (ME)
Nac1
Oct4
B
Oct4-si (ME)
Tcf3
Oct4
C
Oct4-si (ME)
Nanog
Oct4
D
Nac1-si (ME)
Nanog
Nac1
E
Sox2-si (NE)
Oct4
Sox2
F
Sox2-si (NE)
Nac1
Sox2
G
Sox2-si (NE)
Tcf3
Sox2
H
Sox2-si (NE)
Nanog
Sox2
I
Tcf3-si (NE)
Oct4
Tcf3
J
Tcf3-si (NE)
Nac1
Tcf3
K
Tcf3-si (NE)
Sox2
Tcf3
L
Tcf3-si (NE)
Nanog
Tcf3
M
Nac1-si (ME)
Nac1
T
N
Oct4-si (ME)
Oct4
T
O
Sox2-si (NE)
Sox2
Sox1-GFP
P
Tcf3-si (NE)
Tcf3
Sox1-GFP
Q
T (ME)
neg
Oct4−si
Nac1−si
Sox2 (ME)
neg
Oct4−si
Nac1−si
Mean fluorescence (r.f.u.)
R
Exclusive fate choice
Sox1 (NE)
T (ME)
S
Model predictions for key TFs KD
Protein level (a.u.)
WT
Oct4 KD
Tcf3 KD
Sox2 KD
ME
NE
Nac1
Tcf3
Sox2
Oct4

Figure S6

Figure S6: Changes in the TF levels in cells with Nac1 or Oct4 down-regulation during ME, and Sox2 or Tcf3 down-regulation during NE differentiation. Related to Figures 5 and 6.

Nac1 (A), Tcf3 (B) and Nanog (C) levels in cells with siRNA mediated Oct4 down-regulation during ME differentiation. (D) Nanog levels in cells with siRNA mediated Nac1 down-regulation during ME differentiation. Oct4 (E), Nac1 (F), Tcf3 (G) and Nanog (H) levels in cells with siRNA mediated Sox2 down-regulation during NE differentiation. Oct4 (I), Nac1 (J), Sox2 (K) and Nanog (L) levels in cells with siRNA mediated Tcf3 down-regulation during NE differentiation. Changes to single cell level of T upon Nac1 (M) and Oct4 (N) down-regulation during ME differentiation, Sox1-GFP upon Sox2 (O) and Tcf3 (P) down-regulation during NE differentiation. (Q) Box plots showing single cell distributions for changes in T and Sox2 levels when ESCs were transfected with either scrambled siRNA (neg) or target specific siRNA pool during ME differentiation. (R) The mathematical model captured the mutually exclusive ME and NE fate choice, also observed with experimental data (Figure S3H and I). (S) Model predictions for changes in Nac1, Tcf3, Sox2 and Oct4 levels on partial knock-down (KD) of indicated proteins in ME (red) and NE (blue) conditions.

Cells were transfected 12 hrs prior to the addition of signals and measurements were done at 72 hrs of differentiation. TF levels were normalized as in Figures 4, with maximal signals in cells mock-transfected with scrambled siRNA (negative control) under the same experimental conditions. Dashed lines indicate the expected maximum of the indicated protein from mock-transfected cells in ME or NE condition. Increased loss of Nanog with TFs down-regulation during differentiation indicated the augmented loss of non-differentiating portion (ES) of cells (C, D and H). In consistent, Nac1 and Oct4 levels observed with Sox2 down-regulation during NE (E and F) reflected their levels as observed in only the NE positive cells (Figure 3B and D).

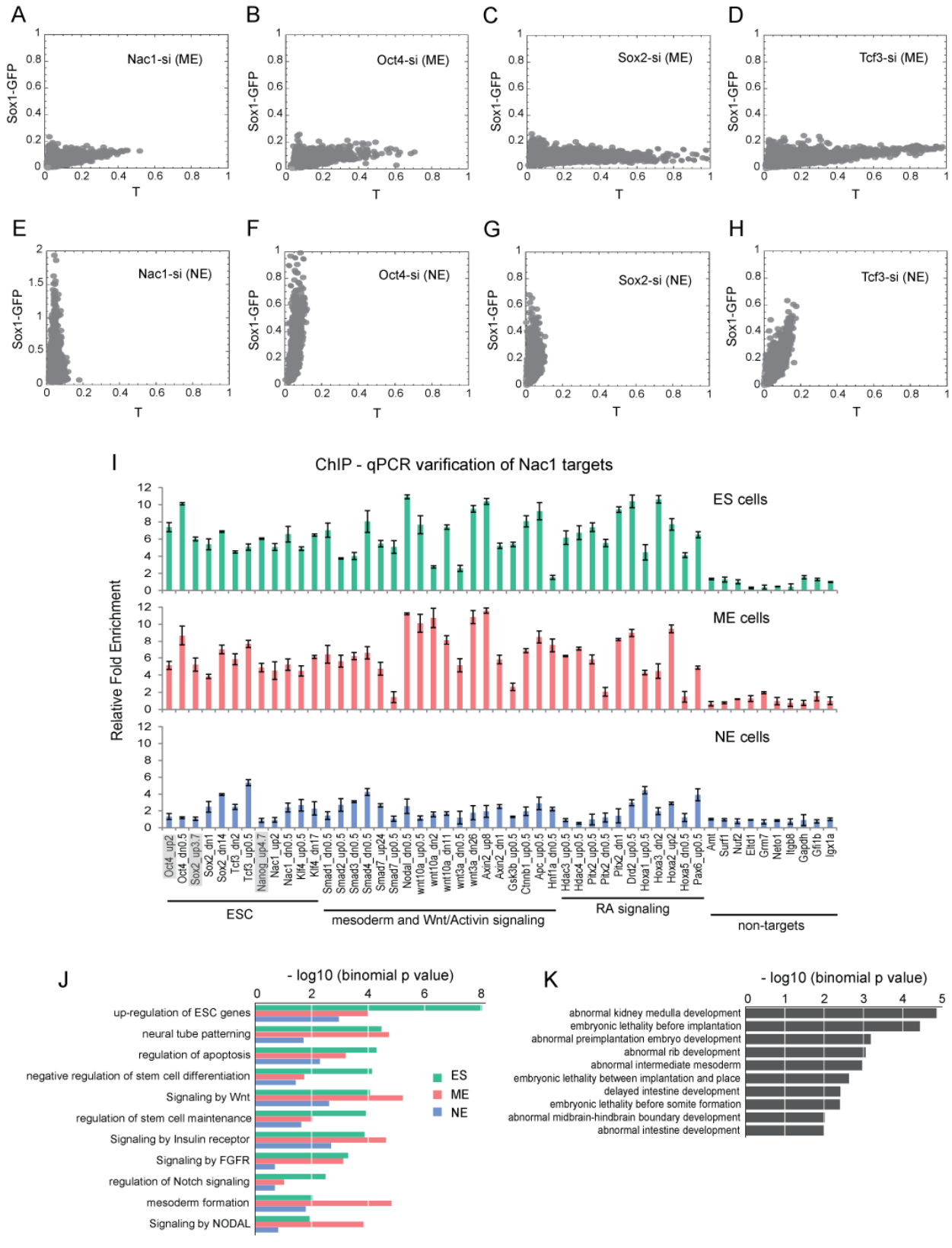
A
Nac1-si (ME)
B
Oct4-si (ME)
C
Sox2-si (ME)
D
Tcf3-si (ME)
E
Nac1-si (NE)
F
Oct4-si (NE)
G
Sox2-si (NE)
H
Tcf3-si (NE)
Sox1-GFP
T
I
ChIP - qPCR varification of Nac1 targets
Relative Fold Enrichment
ES cells
ME cells
NE cells
Oct4_up2
Oct4_dn0.5
Sox2_up3.7
Sox2_dn1
Sox2_dn14
Tcf3_dn2
Tcf3_up0.5
Nanog_up4.7
Nac1_up2
Nac1_dn0.5
Klf4_up0.5
Klf4_dn17
Smad1_dn0.5
Smad2_up0.5
Smad3_dn0.5
Smad4_dn0.5
Smad7_up24
Smad7_up0.5
Nodal_dn0.5
wnt10a_up0.5
wnt10a_dn2
wnt10a_dn11
wnt3a_dn0.5
wnt3a_dn26
Axin2_up8
Axin2_dn1
Gsk3b_up0.5
Ctnnb1_up0.5
Apc_up0.5
Hnf1a_dn0.5
Hdac3_up0.5
Hdac4_up0.5
Pitx2_up0.5
Pitx2_dn0.5
Pitx2_dn1
Drd2_up0.5
Hoxa1_up0.5
Hoxa3_dn2
Hoxa2_up2
Hoxa5_dn0.5
Pax6_up0.5
Amt
Surf1
Nutf2
Eltd1
Grm7
Neto1
Itgb8
Gapdh
Gfi1b
Igx1a
ESC
mesoderm and Wnt/Activin signaling
RA signaling
non-targets
J
- log10 (binomial p value)
up-regulation of ESC genes
neural tube patterning
regulation of apoptosis
negative regulation of stem cell differentiation
Signaling by Wnt
regulation of stem cell maintenance
Signaling by Insulin receptor
Signaling by FGFR
regulation of Notch signaling
mesoderm formation
Signaling by NODAL
ES
ME
NE
K
- log10 (binomial p value)
abnormal kidney medulla development
embryonic lethality before implantation
abnormal preimplantation embryo development
abnormal rib development
abnormal intermediate mesoderm
embryonic lethality between implantation and place
delayed intestine development
embryonic lethality before somite formation
abnormal midbrain-hindbrain boundary development
abnormal intestine development

Figure S7

Figure S7: Analysis of differential Nac1 binding to its targets in ES, ME and NE cells. Related to Figures 6 and 7.

(A - D) Scatter plots showing the single cell quantifications for changes in T and Sox1-GFP levels upon down-regulation of the indicated key TF during ME differentiation.

(E - H) Scatter plots showing the single cell quantifications for changes in T and Sox1-GFP levels upon down-regulation of the indicated key TF during NE differentiation.

Signals were normalized as in Figures 4, with maximal signals in cells mock-transfected with scrambled siRNA (negative control) under the same experimental conditions.

(I) Nac1 targets verification by quantitative PCR (qPCR). Selected Nac1 target loci were verified by site-specific qPCR analysis in ChIP samples from ES, ME and NE cells. qPCR was validated by previously known Nac1 binding on Oct4, Sox2 and Nanog regions (shaded) and non-targets. Y-axis represents the relative fold enrichment of Nac1 binding at the target loci tested from three independent reactions. Fold enrichment is normalized to the negative control Igx1a. Error bars represent standard deviation. (J) Gene ontology and pathway terms enriched among the genes associated with Nac1 binding regions in ES, ME and NE cells. (K) Mouse phenotype terms enriched among the genes associated with Nac1 binding regions in ESCs. Data in (J) and (K) are shown graphically according to their p values (x axis) and the associated functional category (y axis).

SUPPLEMENTAL EXPERIMENTAL PROCEDURES

Embryonic stem cell (ESC) culture

The mouse ESC lines used in this study; R1 (E14-Tg2A), Bry-GFP (Fehling et al., 2003) and Sox1-GFP (Ying et al., 2003), were maintained by culturing on gelatin (0.1%) in Serum-LIF (SL) medium: Knock out DMEM (Gibco, US) supplemented with non-essential amino acids, sodium pyruvate, L-Glutamine, β-mercaptoethanol, 15% fetal calf serum (Hyclone) and Leukemia Inhibitory Factor (LIF – 1000u/ml) (Millipore # ESG1106). Cell medium was changed daily and cells passaged every two to three days at a dilution of 1 in 10.

ESC differentiation

To differentiate ESCs into either mesendoderm (ME) or neuroectoderm (NE), ESCs were first plated in Serum-LIF medium, on coated 24 well plates, at a density of 12,000/ml. After 24 hrs of incubation, cells were washed twice with 1xPBS (- Cacl2, –MgCl2) and fed with fresh N2B27 (Gibco, US) containing LIF and BMP-4 (Stemgent # 03-0007) as described previously (Ying and Smith, 2003; Ying et al., 2008). After 24 hrs of further incubation, cells were washed twice with 1xPBS and induced with specific differentiation signals using N2B27 (without LIF and BMP-4) as base medium: CHIR99021 (Stemgent # 04-0004-02) with Activin-A (R&D Systems # 338-AC-010) for ME differentiation and Retinoic acid (Sigma) for NE differentiation (Sterneckert et al., 2010; ten Berge et al., 2008; Thomson et al., 2011; Ying et al., 2003). Cells were differentiated for up to 120 hrs (data in Figure 1B and C), 96 hrs (for data in Figure 1D and E) or 72 hrs as indicated. Differentiation medium was replaced daily to reduce the influence of increased concentration of secreted factors. Samples for quantitative immuno-fluorescence were taken at indicated time points.

In order to estimate the optimal differentiation conditions, we first tested different concentrations of ME and NE inducing signals (Fig. S1B - C) by using an ES cell line stably expressing Sox1-GFP which has been shown to identify cells adopting the NE fate (Ying et al., 2003). We simultaneously measured Sox1-GFP, Nanog and Brachyury (T) protein levels at 84 hrs of differentiation (Thomson et al., 2011). While the GFP signal was used to measure Sox1 levels, immunostaining of the same cell populations was used to measure Nanog and T levels. Nanog is

generally regarded as a marker of pluripotency (Chambers et al., 2007; Kalmar et al., 2009; Silva and Smith, 2008), and T has been shown to identify cells adopting the ME fate (Gadue et al., 2006). We used changes in T and Sox1 levels as outputs to estimate the changes in ME and NE fates respectively. Quantitatively, while Nanog levels steadily decreased in both fates, T and Sox1 marker levels increased with increasing ME and NE signal concentrations respectively (Fig. S1B - C). At the maximum concentrations, however, both T and Sox1 signals decreased, which might be due to increased cell death observed, especially with RA, or other unintended effects at these concentrations. Changes in the proportion of ES, ME and NE cells at increasing concentrations reflected the changes in their respective marker levels (Fig. S1D - E). Although a minor proportion of ME and NE cells was observed at zero or low signal concentrations, the cell fates remained mutually exclusive. These results indicated that ME cell fate was maximal at 3uM of CHIR and 100ng/ml of Activin, and NE cell fate was maximal at 500nM of RA, without significant cell death. Hence, we used these signal concentrations to respectively induce the ME and NE cell fates.

Perturbations

TF down-regulation using siRNA

We used siRNA perturbation to test the functional significance of key TFs identified through PCA and DBN data analysis. We used the ON-TARGET plus SMART pool siRNA from Dharmacon (Thermo scientific). Each SMART pool included up to four siRNA constructs specific to different regions of a given target. The pooling strategy allowed us to efficiently knock-down the expression levels of Nac1, Oct4, Tcf3, Sox2, Klf4 and Nanog. We validated the siRNAs for their effects of ESC survival and their efficiency in down-regulating the target gene. Three days after transfection, the target protein levels were significantly reduced, as measured by the immuno-fluorescence of the target protein specific antibody (Figure S5A – F). Prolonged incubation, up to six days, severely compromised the ES survival (with Nanog, Sox2, Oct4 and Nac1 knock-out), as measured by the alkaline phosphatase colony assay (Figure S5H). Transfection of siRNAs was performed using DharmaFECT reagent (Thermo Scientific) by following the manufacturer instructions. Cells were transfected in 24 well plates with a final concentration of 25nM of SMART pool siRNA for each target. Mock-transfection with similar concentrations of scrambled siRNA pool was used as negative controls.

In order to down-regulate TFs during the ME and NE differentiation process, siRNA transfection was performed after 24 hrs of incubation in N2B27 containing LIF and BMP-4. Cells were incubated with transfection reagent with either the scrambled SiRNA pool or the indicated target siRNA pool for 12 hrs, washed twice with 1xPBS followed by the addition of N2B27 medium containing either ME or NE specific differentiation signals. Cells were allowed to differentiate for 72 hrs before fixing and processing for immuno-fluorescence assays.

Sequence for siRNA constructs:

Nac1: CAGAUGAGCAGUACCGUCA, GAAUAAACAAGACGCCUUU, CCACAAUGAAGAGGACGAA and CCACCUUAGUCACGAGCUA.
Oct4: CAAGGGAGGUAGACAAGAG, UCACUCACAUCGCCAAUCA, GCUCAGAGGUAUUGGGGAU and GAGAAAGCGAACUAGCAUU.
Kl4: AGAUUAAGCAAGAGGCGGU, CCAUUAUUGUGUCGGAGGA, CCGAGGAGUUCAACGACCU and CGACUAACCGUUGGCGUGA.
Tcf3: GAUCUGAGGUUAAUGGCUC, GGGCCAGUCUUUUGCAUAA, AGAGGCGUAUGGCCAAUAA and CCGGAUCACUCCAGCAAUA.
Nanog: GCUAUAAGCAGGUUAAGAC, GAACUACUCUGUGACUCCA, CAAGAACUCUCCUCCAUUC and CCAGUGAUUUGGAGGUGAA.
Sox2: GGACAGCUACGCGCACAUG, GCUCGCAGACCUACAUGAA, GCACCCGGAUUAUAAAUAC and GAAGAAGGAUAAGUACACG.

Over-expression of TFs

Rescue of TF levels during differentiation (Figure 4E – H) was achieved through their ectopic over-expression from pmCherry-N1 vector containing CMV promoter. Individual TF plasmid constructs were co-transfected with siRNA, using DharmaFECT reagent (Thermo Scientific), 12 hrs prior to the addition of differentiation signal. To over-express Nac1 during NE differentiation (Figure 6H), pN1-Nac1-mCherry construct was transfected using Lipofectamine 2000 for 12 hrs before inducing the differentiation. Expression of the Nac1-mCherry fusion was driven by CMV promoter. Transfected positive cells were detected by imaging the Nac1-mCherry fusion protein.

Alkaline phosphatase assay

We used the alkaline phosphatase (AP) based ES colony assay to assess the effects of ON-TARGET plus SMART pool siRNAs (Figure S5G) on ESCs survival. We used the AP detection kit (Millipore # SCR004) and followed the manufacturer instructions. Briefly, triplicates for each sample in 24 well plate were fixed for 2 minutes with 4% formaldehyde, rinsed with 1x TBST (20mM Tris-Hcl, pH 7.4, 0.15M NaCl, 0.05% Tween-20), incubated with Naphthol/fast red violet solution in dark at room temperature for 15 minutes. Colonies were rinsed with 1x TBST and covered with 1x PBS, imaged and number of red violet colonies were counted.

Quantitative immuno-fluorescence

Immuno-fluorescence

Immuno-fluorescence method was adapted from previously described methods (Kalmar et al., 2009; Munoz Descalzo et al., 2012). ESCs were grown on tissue culture treated plastic or coverslips in 24 well plates and fixed with 4% paraformaldehyde in BBS (50mM BES Sodium salt, 280mM NaCl, 1.5mM Na_2KPO_4 and pH 6.96) with 1mM $CaCl_2$ for 15 minutes. Cells were then washed thrice and blocked with BBT-BSA buffer (BBS with 0.5% BSA, 0.1% Triton and 1mM $CaCl_2$) for 45 minutes at room temperature. Cells were incubated in a humid chamber, at 4°C for overnight with primary antibodies, washed thrice with BBT-BSA and incubated with fluorophore-conjugated secondary antibodies for 1 – 2 hrs in dark and at room temperature. Cells were then washed with BBS – CaCl2, stained for DAPI, mounted using vectashield and imaged.

Primary antibodies used have been either validated in the literature or in this study (MacArthur et al., 2012; Munoz Descalzo et al., 2012; Thomson et al., 2011): Nanog (eBioscience 14-5761, 1:300), Sox2 (Santa Cruz sc-17320, 1:300; Cell Signaling 4900, 1:500), Oct4 (Santa Cruz sc-5279, sc-8628, 1:300), Nac1 (Abcam ab29047, 1:600), Tcf3 (Santa Cruz sc-8635, 1:300), Klf4 (Santa Cruz sc-20691, 1:300), Rex-1(Santa Cruz sc-50670, 1:300; Abcam ab28141, 1:600), Dax1 (Santa Cruz sc-841, 1:300), cMyc (Santa Cruz sc-764, 1:300), Zfp281 (Abcam ab101318, 1:600), Brachyury (Santa Cruz sc-17743, 1:300), Tbx3 (Santa Cruz sc-17871, 1:300), Klf5 (Santa Cruz sc-12998, 1:300) and p53 (Santa Cruz sc-6243, 1:300). Secondary antibodies conjugated to either Alexa 488, 568 or 647 flourophores (Molecular probes, Life technologies) were used at 1:500 dilution.

For the initial data collection with all proteins under ME and NE differentiation conditions (Figure 1D and E), proteins were stained in combinations of three with Oct4 being common in all combinations (Figure S1). Up to eight combinations were created to accommodate all 13 proteins. All the combinations were stained and imaged with cells taken at every 8th hour, up to 96 hrs from the onset of differentiation.

Imaging

Images were acquired with a Nikon Ti motorized inverted microscope fitted with perfect focus and Yokagawa CSU-X1 spinning disk confocal systems, 20x Plan-Apochromatic objective (NA .75) and with Hamamatsu ORCA-AG cooled CCD camera. While Lumencor SOLA fluorescence light source was used to excite DAPI, Spectral Applied Research LMM-5 laser merge module with AOTF controlled solid state lasers: 488nm (100mW), 561nm (100mW) & 642nm (101mW) was used to excite 488, 568 and 647 flourophores respectively. QUAD 405/491/561/642 dichroic mirror along with 525/50, 620/60 and 700/75 filters were used respectively for 488, 568 and 647 fluorophore emission collection (Chroma technologies). 395/25 Excitation and 460/25 emission filters were used for DAPI (Chroma technologies). Images were acquired using MetaMorph software.

Image analysis and fluorescence quantification

Qualitative analysis of images to capture the co-localization of a protein with respect to the ME (Brachyury) and NE (Sox1) fate marker or other proteins was carried out using either Fiji (Image J) or MetaMorph software. Gamma, brightness, and contrast were adjusted on displayed images (identically for compared image sets).

Fluorescence intensities were quantified by semi-automated image analysis through Cell Profiler software (Broad Institute) (Carpenter et al., 2006). A custom Cell Profiler pipeline was created for image analyses. Images were segmented and individual cells were identified using DAPI signals. Similar results were observed, with ME or NE positive cells, in tests with segmentations using either Brachyury (for ME) or Sox1 (for NE) signals. In order to avoid large variations of a given protein in multiple stainings and across different conditions, we chose to quantify the

"*mean fluorescence intensity*" instead of total fluorescence from individual cells. Mean fluorescence was extracted for each of the multiple fluorophore probes used in a given staining.

Normalization

In order to capture the quantitative differences in protein levels across different cell populations we performed max normalization of data collected under identical conditions (immuno-fluorescence, imaging and batch of experiments).

To understand the dynamic changes to protein levels during differentiation process (Figure 1D and E), medians of protein level across all time points were normalized to their maxima under a specific differentiation condition (i.e. ME or NE).

To better visualize varying protein levels across undifferentiated (ESCs), ME and NE cells, single cell data of a give protein was normalized across all three conditions by the signal from a condition where it was maximum. Specifically, we did the following.

1. Nac1, Oct4, Sox2, Nanog, Klf4, Esrrb, Sall4, Smad1 and E2f1 were maximal in undifferentiated ESCs under pluripotency condition and hence their data across all conditions were normalized to their respective maxima in ESCs (Figures 3, S3 and S4).
2. The Tcf3 level was maximal in the NE differentiation condition. Hence, its maximum under the NE condition was used to normalize its expression across all conditions.
3. The maximum signal of Brachyury (ME marker) observed under the ME differentiation condition was used to normalize its expression across all conditions.
4. Similarly, the maximum signal of Sox1 (NE marker) observed under the NE differentiation condition was used to normalize its expression across all conditions.
5. In siRNA mediated perturbation experiments (Figures 4, 5 and 6), similar max-normalization was employed but by using the maximal signals from cells mock-transfected with scrambled siRNA pool (negative control), maintained in ES condition (for TFs) or subjected to ME (for T) or NE (for Tcf3 and Sox1) differentiation.
6. In the TFs rescue experiments (Figures 4 and 6), data was similarly normalized to the maximal signals from ESCs mock-transfected with scrambled siRNA pool and or an empty plasmid, maintained in ES condition or subjected to ME or NE differentiation.

Flow cytometry

For flow cytometry data shown in Figure 6H, Sox1-GFP ESCs were harvested by trypsinization, washed twice with PBS and resuspended in PBS at $2x10^6$ cells per sample. Cells were then filtered to remove aggregates and fluorescence data was collected immediately on a BD LSRII flow cytometer equipped with 405 nm, 488 nm, 561 nm, and 633 nm lasers. Flow cytometry data was analyzed using FlowJo.

Chromatin Immunoprecipitation

Chromatin immunoprecipitation (ChIP) for Nac1 followed by next-generation sequencing (ChIP-Seq) was used to analyze Nac1 binding to the regulatory regions of its targets including other key TFs (Oct4, Sox2, Tcf3, Nanog and Nac1 itself). ChIP followed by quantitative PCR (ChIP-qPCR) was used to validate the targets identified in ChIP-Seq analysis. ChIP was performed using the Magna ChIP reagents (Upstate # 17-409) and by following the manufacturer guidelines. Approximately 10^6 of ESCs grown with LIF and BMP4 and FACS sorted T-GFP and Sox1-GFP positive cells (at 72 hrs of differentiation) were used to perform ChIP. Cells were fixed with 1% formaldehyde, lysed, and the chromatin was sheared using Vibra Cell Sonicator (Sonics) at 60% power for 7 cycles of 15 seconds sonication followed by 50 seconds incubation on ice. Nac1 ChIP was performed using 3µg of antibody (Abcam ab29047). Separate CHIP for a positive control - anti-polymerase II (Upstate 05-623B) and a negative control - normal mouse IgG (Upstate 12-317B) were performed.

ChIP-Seq analysis: Next-generation sequencing was performed using Illumina HiSeq2500 with 50 cycles. Sequences from the Nac1 ChIP-seq were aligned against National Center for Biotechnology Information Build 37 (mm9) of mouse genome using Bowtie (Langmead et al., 2009), allowing up to two mismatches. Only reads that were uniquely mapped to the genome were preserved. ChIP data were compared to input chromatin and peaks were called by MACS (version 1.4.1) with p value cutoff of $1e^{-05}$ (Zhang et al., 2008). Nearest genes and TSS were assigned to peaks by GREAT (McLean et al., 2010) and ChIP-Enrich (Welch et al., 2014). Motif discovery and the significance of discovered motifs were performed using DREME (Bailey, 2011) and TOMTOM (Gupta et al., 2007) respectively. The gene ontology and pathway enrich analyses were performed using GREAT (McLean et al., 2010) and ChIP-Enrich (Welch et al.,

2014). The ChIP-seq sequences for Oct4, Nanog, Sox2, Klf4, cMyc, E2f1 and Zfx were obtained from (Chen et al., 2008) and were subjected to similar analysis to identify their target genes, and profile them against Nac1 targets.

ChIP-qPCR

Selected Nac1 binding targets were validated and its differential binding to these sites was verified by qPCR analysis with ChIPed DNA from ES, ME and NE cells (Figure S7). Known Nac1 binding sites for Oct4, Sox2 and Nanog were used to validate the ChIP-qPCR (Kim et al., 2008). qPCR was performed in triplicates on CFX96 RT-System (Bio-Rad) using the RT2 SYBR Green Fluor (Qiagen #330510). Ct values were first normalized to the input and then to the normal mouse IgG (negative control) to calculate fold enrichment ($2^{\Delta\Delta Ct}$). Relative fold enrichment was calculated over negative control Igx1a (ORF free intergenic region). The primers used for qPCR analysis are listed in the below table.

ChIP-qPCR primer sequences

Primer name	Gene	Approximate distance from TSS	Forward sequence	Reverse sequence	Qiagen ID
Amt_dn1	Amt	downstream 1kb	CTAATCTGCGGAGTGGCTCTT	CCTCACCTGGGTTAGCTGTAGT	
Apc_up0.5	Apc	upstream 0.5kb	TGCTGCGGCTGCGCAGTCCAAT	AGCTCCCCCAAGGTAGCGGCCGGGT	
Axin2_dn1	Axin2	downstream 1kb	TGCGAGGTCTCCGCAAGGAGT	CCGAGCCCGCCGCTTCCCCT	
Axin2_up8	Axin2	upstream 8kb	AGGTAGGAACGTGTTTGATTTGATGGA	ATTTCATGTTTCAAGTTCTCCAGCCTCT	
Ctnnb1_up0.5	Ctnnb1	upstream 0.5kb	TCGCTCCTTGTGCGGCGCCATCT	ACCTCAGGCCCGCGCGCTGCTCA	
Drd2_up0.5	Drd2	upstream 0.5kb	CTCCCGCCCCGCCTCGCCCTG	CGCATCCACGCACGGCCGCCCCT	
Eltd1-dn1	Eltd1	downstream 1kb	CGTCACAGGGGACAGAGCGA	CTAGAAGCGGGAGGAGTCTCA	
Gapdh_dn1	Gapdh	downstream 1kb	TGGTGAAGACACCAGTAGACTCCA	TGGTCTACATGTTCCAGTATGA	
Gfi1b_dn1	Gfi1b	downstream 1kb	CGCCAGATTTTGACACAAATAA	CTGCACAGACAGACACTTCTCC	
Grm7_dn1	Grm7	downstream 1kb	TCCCCTGCTGCGTGCTGGAGGT	TCTCCCTCTTGATGTCGCCGCA	
Gsk3b_up0.5	Gsk3b	upstream 0.5kb	TCGCACAGAGCAGCCCCCGACC	TGCTCGGGAAGTGTCCGCGCTGT	
Hdac3_up0.5	Hdac3	upstream 0.5kb	TCCTCCCGCACAACCCTGAGCCCT	AGGCTGCGTGCTTGCGCAGCACGCA	

Hdac4_up0.5	Hdac4	upstream 0.5kb	TACGCCCGTCAGGCGCCCCAG	TCTCGGACCAATGGAAGGGCGGCT	
Hnf1a_dn0.5	Hnf1a	downstream 0.5kb	TCAAGCTCTGTGGGCACCCCCAG	TGCACTTGCAAGGCTGAAGTCCA	
Hoxa1_up0.5	Hoxa1	upstream 0.5kb	TCAGTGTAGGTGACGCGCGCT	AGGGGGCCTCCCATCCCCCCACA	
Hoxa2_up2	Hoxa2	upstream 2kb	TCCCCGAGACCTGGGGCCAAGT	AGCCCCGCGGGCAGTCGCGGCA	
Hoxa3_dn2	Hoxa3	downstream 2kb	TGCGGGGCGCTCTGGGGCCGCGGGT	ACCGCGAGAAAAATTAGTATTTTTGCA	
Hoxa5_dn0.5	Hoxa5	downstream 0.5kb	TCGGCGGGCGCCGCACTGGCCCCA	TGGAGATCATAGTTCCGTGAGCGA	
Igx1a	Igx1a		n/a	n/a	GPM10000C(-)
Itgb8_dn1	Itgb8	downstream 1kb	TCGACAGGCCGGGTTGGCCGAC	TTGCTTCGCCCCCGCGGGCCAT	
Klf4_up0.5	Klf4	upstream 0.5kb	TCGCTCTCTTGGCCGGGGAACT	ATTTAGCTACCATGGCAACGCGCAGT	
Klf4_dn17	Klf4	downstream 17kb	TCGGCTCTTCCGCCAGCCACACCCT	AGTGAGCATCGGGCTCCGCCTGGAGT	
Nac1_up2	Nacc1	upstream 2kb	n/a	n/a	GPM1054292(-)
Nac1_dn0.5	Nacc1	downstream 0.5kb	AGATTCGGCCATCTCACTCTTGCCCT	AGCGCAGGTGAGATGGCCCGCCCCA	
Nanog_up4.7	Nanog	upstream 4.7kb	AATGAGGTAAAGCCTCTTTTT	ACCATGGACATTGTAATGCAAA	
Neto1_dn1	Neto1	downstream 1kb	AGAGAGGAGGGCTGCGGCTGGA	TGTGAGAGGCAGAAGGCGCA	
Nodal_dn0.5	Nodal	downstream 0.5kb	TGCCTCTGTGGACACGGGGGCA	TCCCGGCCGTGAGCCCTTAAGTGCT	
Nuf2_dn1	Nuf2	downstream 1kb	TAGGGACATAAAAGCTGTACACGT	TTAGATCCTTTCTACCCAGGCCCA	
Pax6_up0.5	Pax6	upstream 0.5kb	AGGCAGGCGGCTGGCTCTGCA	AAGCATCGCCGGCGGCTGCTCT	
Pitx2_up0.5	Pitx2	upstream 0.5kb	TGGAGTTTGGTGGAATCTCTGCT	AGGGTCCACGCGGGGGGCTGCTAAA	
Pitx2_dn0.5	Pitx2	downstream 0.5kb	AGGGAGGGAGGCAAGAAAAGGGTCT	TGTCTCCTCTAGCTTCAGACTCCA	
Pitx2_dn1	Pitx2	downstream 1kb	TCGAGTTCACGGACTCTCCCAA	TGGCAGCTTCGCCCGCCCGTGCT	
Oct4_up2	Pou5f1	upstream 2kb	n/a	n/a	GPM1033119(-)
Oct4_dn0.5	Pou5f1	downstream 0.5kb	TTCTGCGGAGGGATGGCATACTGT	TTCCACCTTCTCCAACTTCACGGCA	
Smad1_dn0.5	Smad1	downstream 0.5kb	ACACAATGGGGCTGCGGCCCGAT	ACCCGCGCTGAAGGAAATCTGGGA	
Smad2_up0.5	Smad2	upstream 0.5kb	TTGGCTGCGCGCGCCGCCGGT	TAGGCGTGAGGCACGCCGGCCGA	
Smad3_dn0.5	Smad3	downstream 0.5kb	ACTGGGGACGCCGGGGGCGCTCA	TCCGGGGCCTGCCCGTCAGTCCGT	
Smad4_dn0.5	Smad4	downstream 0.5kb	TCCGGCCCAGGCGGCCCCCTCT	AGGCCCTTCCCGCGCCGCGCTCCGCT	
Smad7_up24	Smad7	upstream 24kb	ACCTTCGCCACCCTGTGGCTCGCA	AGGGGGAGCTTTGAGCGCGGCCGGGT	
Smad7_up0.5	Smad7	upstream 0.5kb	ACGGCCACGTGACGAGGCCGGA	AGGGCTCGCCGCCTCCCGCA	
Sox2_dn1	Sox2	downstream 1kb	AGCGGCGTAAGATGGCCCAGGAGA	TGCTCCTTCATGTGCAGAGCGCGCA	

Sox2_dn14	Sox2	downstream 14kb	TAAAACGTGCACCCCGCCGAGTGTT	AGATAATTCTCTGCACTCAGCGCCGA	
Sox2_up3.7	Sox2	upstream 3.7kb	GCAATGCTGAGAAATTCCAGTT	GTTCCCCTCCTCTCCTAATCTC	
Surf1_dn1	Surf1	downstream 1kb	CAAGAAGTACCAACGGCTGTC	GCCAAACTACGTACCGATTCTTT	
Tcf3_up0.5	Tcf3	upstream 0.5kb	CCCCTCCGCGTGCGCTCACCTGCT	AGTGGGGAGGAGGAAGGACGCGCGA	
Tcf3_dn2	Tcf3	downstream 2kb	n/a	n/a	GPM1052107(+)
Wnt10a_up0.5	Wnt10a	upstream 0.5kb	AGCCCGCTGCACCTCCTTACCCT	ATGGGGCAGCGCCCCCGGGCA	
Wnt10a_dn2	Wnt10a	downstream 2kb	CCGAGCCCAGCCCGACGCGTGT	CCCAGCTGACAAGAGGGGGTGA	
Wnt10a_dn11	Wnt10a	downstream 11kb	AGCCGCGCCTGGACTCGGCAGGCA	ATTCTTCGCAGACCACGAAGCAGCA	
Wnt3a_dn0.5	Wnt3a	downstream 0.5kb	ATGGACTTTCACTGCCCTCCCT	AGGGCAACCGCCCCCCTGGGGCA	
Wnt3a_dn26	Wnt3a	downstream 26kb	TGGCGCCTCCCCTCCAAGGCT	ACGGTGGGGCACCGGCGCATT	

*TSS: transcription start site

Computational analysis

Principal Components Analysis (PCA)

PCA is a statistical procedure that reduces the multi-dimensionality of the data without compromising its variation (Jolliffe, 2002). To accomplish this, PCA uses orthogonal transformation to convert a set of observations into a set of linear values called the directions or principal components, along which the data variation is maximal. The transformation is defined in a way to account for most of the variability in data along the first principal component. Each successive component is orthogonal to the preceding component and accounts for the highest possible variance in its direction. Hence, the number of principal components is always less than or equal to the number of original variables. The underlying shape of the data may thereby be captured with a few principal components.

For the purpose of PCA analysis, we used the median of the single-cell data for all proteins measured, at all 13 time points and in both ME and NE conditions. We used the median values instead of averages to account for single cell distributions of the data and to avoid the biases that can be caused by segmentation errors or auto fluorescence.

We next centered the matrix of median values by computing the mean value for each protein over all time points and conditions, and subsequently subtracting that value from all the data corresponding to that protein. This is a standard preprocessing step in PCA that removes the primary moment of the data, and ensures that the first principal component corresponds to changes in protein levels, not the absolute levels. As different antibodies are used to probe different proteins, only the relative changes in protein levels over time truly reflect the biology.

PCA was performed using singular value decomposition of the centered matrix into;

$$\boldsymbol{X = U\,D\,V^T}$$

The coordinates of each time point projected onto the principal components were extracted from the columns of **V**, and used to make the PCA plots (Figures 2 and S2). The principal components are defined as linear combinations of each protein; these weights were extracted from the columns of **U**. The "percent variance explained" was computed as a cumulative sum of $\boldsymbol{d_i^2/\Sigma_j (d_j^2)}$, where the $\boldsymbol{d_i}$ are the diagonal entries of the matrix **D**.

Dynamic Bayesian Network (DBN) learning

As a complementary approach to PCA we used Dynamic Bayesian Networks (DBN). Bayesian Networks and related probabilistic models have been widely used to infer likely causal relationships in biological data (Friedman et al., 2000; Pe'er, 2005). A Bayesian Network (BN) is a directed acyclic graph with accompanying probability distributions, in which the "nodes" represent the proteins of interest and the "edges" reflect probabilistic causal relationships (Friedman, 2004; Friedman et al., 2000; Pearl, 2009) (Figure S2N). If there is no edge from node ***i*** to node ***k***, this indicates that the level of protein ***k*** does not directly depend on (is causally independent of) the level of protein ***i***. If there are edges from, for example, nodes ***i*** and j to node ***k***, this indicates that the level of protein ***k*** is conditionally dependent on the levels of protein ***i*** and protein ***j***. That is, there is a joint probability distribution which specifies the conditional probability that protein ***k*** has a particular level, given that proteins ***i*** and ***j*** have particular levels. A DBN adds the element of time and allows protein levels at time point t to depend on protein levels at time point t-1, thereby permitting cycles in the directed graph (Dondelinger, 2013). BN

inference involves a search for a directed graph and joint probability distributions that best fit the observed correlations in the data. To assure computational efficiency, it is helpful to use prior network knowledge to seed or inform the graph structure.

For network inference, we first scaled the median values from ten TFs, Oct4, Sox2, Nanog, Klf4, cMyc, Rex1, Nac1, Dax1, Zfp281 and Tcf3, at all 13 time points by their maximum value under respective ME and NE differentiation conditions. After rescaling, each protein can take values from 0 to 1; this step minimizes any potential bias against low-expressed proteins. We also centered the values as described above.

We applied a custom modified version of the EDISON package (Dondelinger, 2013) in R to learn separate dynamic Bayesian networks from the ME and the NE data. This algorithm uses a Bayesian hierarchical model to score potential network models. The network model is formulated using linear regression. The value of a child node at time "t" is modeled as a linear combination of the values of the parents at time "t-1". In contrast to standard DBN learning, the network structure is allowed to change during the time-course at so-called "change points". EDISON uses a Markov chain Monte Carlo (MCMC) approach to search through the large model space. During the MCMC process, the network structure for any time segment can be altered by adding or removing an edge, and change points can be added, removed or shifted in time.

We note that, we made two small modifications to the EDISON package as downloaded from the CRAN repository to correct minor issues with the running of the software: 1) during any MCMC step involving birth of a change point, we kept the model the same if the maximum number of change points had already been reached, and 2) during MCMC steps involving structure changes, we amended the loop so that it correctly runs through all time segments. We also added the functionality of imposing hard constraints on the network model in the final time segment (described in more detail below).

We first applied the EDISON algorithm using default values for the parameters. We ran the MCMC for 50,000 steps each time. Additionally, in order to test robustness and convergence we

repeated each run 10 times, each time with a different random initial network. During each MCMC run, 1000 instances of the model are sampled after a burn-in 25% of the way through. From these instances, one estimates the posterior probability of change points and network edges. We used all default parameters including imposing a maximum of five parents for each child node and a minimum of two time points between adjacent change points. The final networks were drawn in Cytoscape 3.0.0. Network edges were drawn only if the posterior probability was greater than 0.25.

We then ran EDISON while imposing hard constraints on the edges of the network in the final time segment. This was implemented in the code by 1) keeping the network model of the final segment the same, even if an adjacent change point was created or destroyed and 2) never altering the constrained edge during a network structure change in the final segment. This effectively allows the MCMC process to only traverse the subspace of models that satisfy the hard constraint. In the random prior network that was used for DBN, we imposed the following two constrains that had been well characterized; Oct4 to be a parent node of Sox2 for ME DBN to incorporate known regulation of Sox2 by Oct4 during ME specification (Thomson et al., 2011); Tcf3 to be a parent node of Nanog, Oct4, and Rex1 for DBN on both ME and NE, to incorporate generally known inhibitory functions of Tcf3 (Cole et al., 2008; Pereira et al., 2006; Wray et al., 2011).

Finally, for each of the 1000 network model samples from the MCMC runs, we computed a "dominance score" for each protein (Friedman et al., 2000). We defined the dominance score for protein $\boldsymbol{j}$ as $\boldsymbol{DS_j = \Sigma_i(1/L_{ij})}$ where $\boldsymbol{L_{ij}}$ is the length of the shortest directed path between protein $\boldsymbol{i}$ and protein $\boldsymbol{j}$ in the network . If there is no such path, $\boldsymbol{L_{ij}}$ is defined to be infinite. This score rewards proteins that are directly upstream of many other proteins. We averaged the dominance score over all 1000 samples and over all 10 independent MCMC runs in order to get a final score for each protein, which is represented in the network Figures 2G and H. Dynamic bayesian network code is available for download at https://github.com/meghapadi/StemCellDBN.

Mathematical modelling

In order to gain insights into how the key pluripotent TFs and the Nac1 mediated regulations operate to determine ME or NE choice, we built a simple mathematical model. The model considered most of the observations made through experimental results of this study and consists of four interacting species: Nac1 (**N**), Tcf3 (**T**), Sox2 (**S2**) and Oct4 (**O**). The following regulations among these four TFs were considered based on experimental data in figures 5 & S6:

(i) Activation of Oct4 by Nac1

(ii) Inhibition of Tcf3 also by Nac1

(iii) Inhibition of Sox2 by both Nac1 and Oct4

In addition, two modulating signal events are considered based on another set of observations in this study (Figure 3):

(iv) Retinoic Acid (**R**), which inhibits Nac1 and Oct4

(v) Wnt signaling either via Chiron (CHIR) or Wnt3a (**W**), which inhibits Tcf3 activity.

The resulting network displays no feedback loops and hence information flows unidirectionally from the signals to the genes (from left to right as in Figure 5E). Since little is known about the time scale and dynamics of the decision process under study, we took a dimensionless approach by assuming all proteins to be equally stable (same degradation rates) and reported the time developments relative to these degradation rates. This way, we can now describe the dynamics of this network with the following set of ordinary differential equations:

$$\frac{dN}{dt} = b_1 \frac{1}{1+R} - N,$$

$$\frac{dT}{dt} = b_2 \frac{1}{1+\left(\frac{N}{K_2}\right)^2 + W} - T,$$

$$\frac{dS_2}{dt} = b_3 \frac{1}{1+\left(\frac{O \cdot N}{K_3}\right)^2} - S_2,$$

$$\frac{dO}{dt} = b_4 \frac{\left(\frac{N}{K_4}\right)^2}{1+\left(\frac{N}{K_4}\right)^2 + R} - O.$$

Each of the above equation describes the temporal evolution of the protein levels for the four factors (Nac1, Tcf3, Sox2 and Oct4). Activation and inhibition events are described by standard Hill functions with cooperativity exponents 1 or 2 and all species are assumed to decay linearly. The model contains seven parameters; four maximum production rates (b1, b2, b3, b4), two inhibition thresholds (K2, K3), and one activation threshold (K4) that have been manually fitted to the experimental results.

In addition to the four core factors, we also included the two fate marker reporters – Brachyury (T) for ME and Sox1 for NE. In the model, T (**B**) is allowed to be active when both Oct4 and Nac1 levels are high. Similarly Sox1 (**S1**) is allowed to be triggered in the presence of both Sox2 and Tcf3. These attributes of fate markers were described with the following equations:

$$\frac{dB}{dt} = b_5 \frac{\left(\frac{O \cdot N}{K_5}\right)^2}{1 + \left(\frac{O \cdot N}{K_5}\right)^2} - B,$$

$$\frac{dS_1}{dt} = b_6 \frac{\left(\frac{S_2 \cdot T}{K_6}\right)^2}{1 + \left(\frac{S_2 \cdot T}{K_6}\right)^2} - S_1.$$

These two additional variables require four extra parameters (b5, b6, K5 and K6), which have also been fitted manually.

The following table summarizes all the parameter values used in our model

b1	2/3	b4	3/5	K1	0.125	K4	0.2
b2	3/2	b5	1	K2	0.1	K5	0.075
b3	3/5	b6	5/4	K3	0.05	K6	0.175

To mimic the experimental ME and NE differentiation conditions we set the values of input signals to **W** = 10 and **R** = 0 for ME and **W** = 0 and **R** = 5 for NE.

Robustness to initial conditions

Pluripotency is a heterogeneous state where in cells can have varying concentration of protein levels and yet the pluripotent network is held together by their self-re-enforcing positive regulations. By contrast, as cells encounter differentiation signals and move towards adopting a specific fate, the levels of the different factors tend to homogenize in a combinatorial manner. To test whether our model can capture this behavior and the degree of its robustness, we simulated the dynamics for many different initial conditions with disparate levels of the four factors (Nac1, Tcf3, Sox2 and Oct4). In both ME and NE conditions we found that the model always robustly relaxed to the desired optimal steady state (Figure 5F). It is also easy to check by analysis of the equations above that the model has a single steady state for any values of the parameters.

The model contains only seven parameters: four parameters for the maximum transcription rates of each gene, two inhibition thresholds, and one activation threshold. Because the model exhibits a single steady state for all initial conditions, it was easy to manually find parameter values which captured the experimental results. We performed parameter sensitivity analysis, which showed that individual parameter values could be substantially modified (by up to ±25%) without significantly affecting the correspondence with the experimental data (data not shown). The model thus reproduces the experimental results for a wide range of parameter values.

In-silico perturbations

The proposed mathematical model for ME - NE decision making establishes a framework where new predictions can be made. To test how perturbation of a key TF might bias cells ability to choose between ME and NE choice, we systematically knocked down each TF and explored the prediction behavior of the model. To be consistent with experimentally observed siRNA perturbation efficiency (i.e. up to 80%), in the model we modified maximum production rate of a factor to 25% of its value in the wild type. In addition to recapitulating the experimentally observed changes to protein levels, these in-silico perturbation tests made novel predictions for changes in Tcf3 levels and the extent of NE fate choice. These unexpected model predictions further lead us to design new functional verification experiments. The ensuing results allowed us to discover the novel and uniquely dominant role of Nac1 in promoting the ME and inhibiting the NE choice.

SUPPLEMENTAL REFERENCES

Bailey, T.L. (2011). DREME: motif discovery in transcription factor ChIP-seq data. Bioinformatics *27*, 1653-1659.

Carpenter, A.E., Jones, T.R., Lamprecht, M.R., Clarke, C., Kang, I.H., Friman, O., Guertin, D.A., Chang, J.H., Lindquist, R.A., Moffat, J., *et al.* (2006). CellProfiler: image analysis software for identifying and quantifying cell phenotypes. Genome biology *7*, R100.

Chambers, I., Silva, J., Colby, D., Nichols, J., Nijmeijer, B., Robertson, M., Vrana, J., Jones, K., Grotewold, L., and Smith, A. (2007). Nanog safeguards pluripotency and mediates germline development. Nature *450*, 1230-1234.

Chen, X., Xu, H., Yuan, P., Fang, F., Huss, M., Vega, V.B., Wong, E., Orlov, Y.L., Zhang, W., Jiang, J., *et al.* (2008). Integration of external signaling pathways with the core transcriptional network in embryonic stem cells. Cell *133*, 1106-1117.

Cole, M.F., Johnstone, S.E., Newman, J.J., Kagey, M.H., and Young, R.A. (2008). Tcf3 is an integral component of the core regulatory circuitry of embryonic stem cells. Genes & development *22*, 746-755.

Dondelinger, F., Lebre, S., Husmeier, D. (2013). Non-homogeneous dynamic Bayesian networks with Bayesian regularization for inferring gene regulatory networks with gradually time-varying structure. Machine Learning *90*, 191-230.

Dunn, S.J., Martello, G., Yordanov, B., Emmott, S., and Smith, A.G. (2014). Defining an essential transcription factor program for naive pluripotency. Science *344*, 1156-1160.

Fehling, H.J., Lacaud, G., Kubo, A., Kennedy, M., Robertson, S., Keller, G., and Kouskoff, V. (2003). Tracking mesoderm induction and its specification to the hemangioblast during embryonic stem cell differentiation. Development *130*, 4217-4227.

Friedman, N. (2004). Inferring cellular networks using probabilistic graphical models. Science *303*, 799-805.

Friedman, N., Linial, M., Nachman, I., and Pe'er, D. (2000). Using Bayesian networks to analyze expression data. Journal of computational biology : a journal of computational molecular cell biology *7*, 601-620.

Gadue, P., Huber, T.L., Paddison, P.J., and Keller, G.M. (2006). Wnt and TGF-beta signaling are required for the induction of an in vitro model of primitive streak formation using embryonic stem cells. Proceedings of the National Academy of Sciences of the United States of America *103*, 16806-16811.

Gupta, S., Stamatoyannopoulos, J.A., Bailey, T.L., and Noble, W.S. (2007). Quantifying similarity between motifs. Genome biology *8*, R24.

Jolliffe, I.T. (2002). Principal Component Analysis (New York: Springer).

Kalmar, T., Lim, C., Hayward, P., Munoz-Descalzo, S., Nichols, J., Garcia-Ojalvo, J., and Martinez Arias, A. (2009). Regulated fluctuations in nanog expression mediate cell fate decisions in embryonic stem cells. PLoS biology *7*, e1000149.

Kim, J., Chu, J., Shen, X., Wang, J., and Orkin, S.H. (2008). An extended transcriptional network for pluripotency of embryonic stem cells. Cell *132*, 1049-1061.

Langmead, B., Trapnell, C., Pop, M., and Salzberg, S.L. (2009). Ultrafast and memory-efficient alignment of short DNA sequences to the human genome. Genome biology *10*, R25.

MacArthur, B.D., Sevilla, A., Lenz, M., Muller, F.J., Schuldt, B.M., Schuppert, A.A., Ridden, S.J., Stumpf, P.S., Fidalgo, M., Ma'ayan, A., *et al.* (2012). Nanog-dependent feedback loops regulate murine embryonic stem cell heterogeneity. Nature cell biology *14*, 1139-1147.

McLean, C.Y., Bristor, D., Hiller, M., Clarke, S.L., Schaar, B.T., Lowe, C.B., Wenger, A.M., and Bejerano, G. (2010). GREAT improves functional interpretation of cis-regulatory regions. Nature biotechnology *28*, 495-501.

Munoz Descalzo, S., Rue, P., Garcia-Ojalvo, J., and Martinez Arias, A. (2012). Correlations between the levels of Oct4 and Nanog as a signature for naive pluripotency in mouse embryonic stem cells. Stem cells *30*, 2683-2691.

Pe'er, D. (2005). Bayesian network analysis of signaling networks: a primer. Science's STKE : signal transduction knowledge environment *2005*, pl4.

Pearl, J. (2009). Causality: Models, Reasoning and Inference, 2 edn (Cambridge, UK: Cambridge University Press).

Pereira, L., Yi, F., and Merrill, B.J. (2006). Repression of Nanog gene transcription by Tcf3 limits embryonic stem cell self-renewal. Molecular and cellular biology *26*, 7479-7491.

Silva, J., and Smith, A. (2008). Capturing pluripotency. Cell *132*, 532-536.

Sterneckert, J., Stehling, M., Bernemann, C., Arauzo-Bravo, M.J., Greber, B., Gentile, L., Ortmeier, C., Sinn, M., Wu, G., Ruau, D., *et al.* (2010). Neural induction intermediates exhibit distinct roles of Fgf signaling. Stem cells *28*, 1772-1781.

ten Berge, D., Koole, W., Fuerer, C., Fish, M., Eroglu, E., and Nusse, R. (2008). Wnt signaling mediates self-organization and axis formation in embryoid bodies. Cell stem cell *3*, 508-518.

Thomson, M., Liu, S.J., Zou, L.N., Smith, Z., Meissner, A., and Ramanathan, S. (2011). Pluripotency factors in embryonic stem cells regulate differentiation into germ layers. Cell *145*, 875-889.

Welch, R.P., Lee, C., Imbriano, P.M., Patil, S., Weymouth, T.E., Smith, R.A., Scott, L.J., and Sartor, M.A. (2014). ChIP-Enrich: gene set enrichment testing for ChIP-seq data. Nucleic acids research *42*, e105.

Wray, J., Kalkan, T., Gomez-Lopez, S., Eckardt, D., Cook, A., Kemler, R., and Smith, A. (2011). Inhibition of glycogen synthase kinase-3 alleviates Tcf3 repression of the pluripotency network and increases embryonic stem cell resistance to differentiation. Nature cell biology *13*, 838-845.

Ying, Q.L., and Smith, A.G. (2003). Defined conditions for neural commitment and differentiation. Methods in enzymology *365*, 327-341.

Ying, Q.L., Stavridis, M., Griffiths, D., Li, M., and Smith, A. (2003). Conversion of embryonic stem cells into neuroectodermal precursors in adherent monoculture. Nature biotechnology *21*, 183-186.

Ying, Q.L., Wray, J., Nichols, J., Batlle-Morera, L., Doble, B., Woodgett, J., Cohen, P., and Smith, A. (2008). The ground state of embryonic stem cell self-renewal. Nature *453*, 519-523.

Zhang, Y., Liu, T., Meyer, C.A., Eeckhoute, J., Johnson, D.S., Bernstein, B.E., Nusbaum, C., Myers, R.M., Brown, M., Li, W.*, et al.* (2008). Model-based analysis of ChIP-Seq (MACS). Genome biology *9*, R137.